



Mn-doped zirconium metal-organic framework as an effective adsorbent for removal of tetracycline and Cr(VI) from aqueous solution

Zhao-hui Yang^{a,b,*}, Jiao Cao^{a,b}, Yu-peng Chen^{a,b}, Xin Li^{a,b}, Wei-ping Xiong^{a,b}, Yao-yu Zhou^c, Cheng-yun Zhou^{a,b}, Rui Xu^{a,b}, Yan-ru Zhang^{a,b}

^a College of Environmental Science and Engineering, Hunan University, Changsha 410082, PR China

^b Key Laboratory of Environmental Biology and Pollution Control (Hunan University), Ministry of Education, Changsha 410082, PR China

^c College of Resources and Environment, Hunan Agricultural University, Changsha 410128, PR China

ARTICLE INFO

Keywords:
UiO-66
Mn-doped
Adsorption
Tetracycline
Cr(VI)

ABSTRACT

Metal-organic frameworks (MOFs) with porous property have gained much concern in environment remediation. Herein, the Mn-doped UiO-66 (denoted as MnUiO-66) with cubic morphology was fabricated with a facile solvothermal method. To investigate the adsorption performance of MnUiO-66, tetracycline (TC) and Cr(VI) were chosen as the target pollutant. The maximum adsorption capacity of MnUiO-66 for TC and Cr(VI) were 184.493 mg g⁻¹ and 32.773 mg g⁻¹, respectively, which were 4.9 and 3.1 times higher than the pristine UiO-66. Effects of the solution pH values, initial concentrations and coexisting ions on adsorption capacity were investigated and the adsorption mechanism based on zeta potential measurement was proposed. The adsorption process of MnUiO-66 over TC and Cr(VI) had the most accordance with pseudo-second-order and Langmuir models, which suggested that chemisorption was dominant in adsorption reaction and the MnUiO-66 adsorbent had a homogenous surface for adsorption. Adsorption thermodynamic studies implied that the adsorption process of TC and Cr(VI) on MnUiO-66 were spontaneous and exothermic. In addition, the MnUiO-66 showed excellent adsorption performance in TC-Cr(VI) mixed sample and pharmaceutical wastewater. More importantly, the regeneration experiment indicated the MnUiO-66 adsorbent was recyclable. This work provided a useful insight into the fabrication MOFs-based adsorbent for water purification.

1. Introduction

Water pollution has become a global and inevitable question in the last decades. Large amounts of wastewater are discharged into aqueous environment and bring out negative environmental effects. Notably, antibiotics and heavy metal ions are regarded as the major pollutants in wastewater [1]. Once they enter into the hydrological cycle system, they will result in serious consequences. Currently, the adsorption method has been applied to wastewater treatment and gained considerable concentration for the high removal efficiency, low cost and simple operation [2,3].

Metal-organic frameworks (MOFs) are metal coordination networks with organic ligands containing potential voids, as the IUPAC definition [4]. Since the MOFs were formally reported by Yaghi in 1995 [5], this kind of inorganic-organic hybrid materials have attracted worldwide attention in the past decades. MOFs with porous property have been applied in adsorption of contaminants removal in aqueous. Compared to the traditional inorganic porous adsorbents (for instance, zeolite and

activated carbon), MOFs have some unique advantages, such as ultra-high BET surface area (even reached to 7000 m² g⁻¹ [6]), high/tunable porosity, various pore functionality and structures, open metal sites, and so on. A large number of researchers have explored the application of MOFs for removing hazardous contaminants in aqueous environment. Haque et al. [7] firstly applied MIL-101 (Cr) and MIL-53 (Cr) in adsorption removal of methyl orange (MO). They discovered that higher BET surface area and larger total pore volume were conducive to adsorption ability of MOFs. Tan et al. [8] synthesized MIL-100 (Fe) with supreme methylene blue (MB) adsorption capacity of 1105 mg g⁻¹. Other reports on adsorptive removal of contaminants by MOFs including MO and MB on MOF-235 [9], MO on ZIF-67 [10], nitroimidazole on MIL-53 (Al) [11], Cd(II) on PCN-101 [12], Cu-BTC for Cr(VI) [13] and so on. Since the MOFs have showed great potential in adsorptive removal of contaminants from aquatic environment, it is urgent to synthesis MOF-based adsorbent with other properties.

Structural stability of MOFs is the primary issue for adsorption application in water purification. There are plenty of reports on Zr(IV)-

* Corresponding author. College of Environmental Science and Engineering, Hunan University, Changsha, Hunan 410082, China.
E-mail address: yzh@hnu.edu.cn (Z.-h. Yang).

based MOFs with excellent hydrothermal, chemical and water stability [14,15]. The UiO-66 (names from University of Oslo) with high degree of network connection is formed by linking $[\text{Zr}_6\text{O}_4(\text{OH})_4(\text{CO}_2)_{12}]$ brick structure and twelve terephthalate linkers [16,17]. Notably, the UiO-66 displays structural stability even in acidic ($\text{pH} = 1$), alkaline ($\text{pH} = 14$) [18] and high-temperature (up to 375°C in air) [19]. To our delight, the UiO-66 is stable in water [20]. Hossein Molavi et al. [21] found that the UiO-66 was stable in water after 12 months, as confirmed by the XRD results. As a kind of stable MOFs, UiO-66 shows great adsorption performance in water purification. The reports on UiO-66 adsorptive removal of contaminants in aqueous solution including dyes [21], antibiotics [22], heavy metal ions [23], and so on. Nevertheless, as an adsorbent, there are some disadvantages of UiO-66, for instance, low adsorption capability and long equilibrium time. Large amounts of methods have been used to enhance the adsorption ability. For instance, the UiO-66 was modified with different functional groups (amino and thiourea groups). The functionalized UiO-66, UiO-66-NH₂ and UiO-66-NHC(S)NHMe displayed higher adsorption performance for Cd(II), Hg(II) and Pb(II) than pristine UiO-66. The introduction of functional groups improved the affinity for heavy metal ions [24]. Recently, metal-doped modification has been found to improve the adsorption ability. Yang et al. [25] reported that Ce(III)-doped modification multiplied the active sites of UiO-66 and promoted π - π interactions between dyes and UiO-66 adsorbent [26]. From the above works, manganese (Mn) ion was applied to be doped into UiO-66 framework because that the ionic radius of Mn(II) was similar to Zr(IV) [27].

Herein, we reported a facile synthesis of Mn-doped UiO-66 adsorbent with high adsorption capacity for wastewater treatment. Tetracycline (TC) and Cr(VI), as two kinds of typical contaminants, were chosen as target pollutants to further expand the application of the as-obtained Mn-doped UiO-66 adsorbent. XRD, FESEM, EDS, FT-IR, TGA and BET analyses were applied to analyze the morphology, structure of the Mn-doped UiO-66. The Mn-doped modification greatly enhanced the adsorption performance of UiO-66. On the one hand, the Mn-doped modification caused a larger BET surface area and pore size, which was helpful for the adsorption reaction. On the other hand, the doped Mn element in UiO-66 lattice donated valence electron and caused more adsorptive sites. Plenty of experiments were implemented to test the adsorption properties of Mn-doped UiO-66 and the corresponding mechanisms based on zeta potential measurement were proposed. The adsorption performance of Mn-doped UiO-66 in TC-Cr(VI) mixed sample and pharmaceutical wastewater was estimated, too. Moreover, recyclability of the adsorbent was evaluated. This work provided useful insight into the fabrication of MOF-based adsorbent with high removal efficiency.

2. Experiment

2.1. Materials

1, 4-benzenedicarboxylic acid (H_2BDC), zirconium chloride (ZrCl_4), manganese(II) chloride ($\text{MnCl}_2 \cdot 4\text{H}_2\text{O}$), N,N-Dimethylformamide (DMF; $(\text{CH}_3)_2\text{NCHO}$), ethanol ($\text{C}_2\text{H}_6\text{O}$), tetracycline (TC) and potassium dichromate ($\text{K}_2\text{Cr}_2\text{O}_7$). All the reagents and materials obtained the standard of analytical grade. During the experiments, deionized water was employed as solvent.

2.2. Fabrication of Mn-doped UiO-66

The Mn-doped UiO-66 adsorbent was fabricated through a facile solvothermal process. In detail, H_2BDC , ZrCl_4 , $\text{MnCl}_2 \cdot 4\text{H}_2\text{O}$ and DMF were mixed in a breaker with a molar ratio of 1:1:1:162. The solution was magnetic stirred for 1 h to get a clear solution and then placed in a 100 mL Teflon liner. The solvothermal process was carried out at 120°C for 24 h. The obtained precipitates were centrifuged and washed with

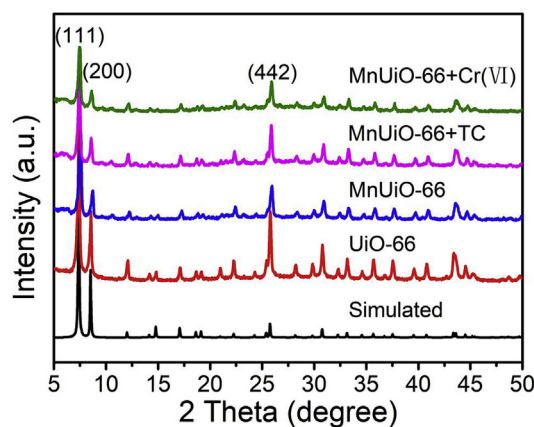


Fig. 1. XRD patterns of UiO-66 and MnUiO-66 samples, and the MnUiO-66 samples after adsorption of TC and Cr(VI).

DMF (removal of redundant H_2BDC) and ethanol (removal of residual DMF). At last, the products were vacuum dried at 60°C . Moreover, the pristine UiO-66 was fabricated without $\text{MnCl}_2 \cdot 4\text{H}_2\text{O}$ on the basis of the above method.

3. Results and discussion

3.1. Characterizations

The constitution and phase composition of the sample could be obtained by X-ray diffractometry (XRD) analysis [28]. As Fig. 1 showed, the characteristic peaks of UiO-66 and MnUiO-66 were in accordance with the simulated UiO-66 pattern, which suggested the UiO-66 crystal was successfully synthesized and the Mn-doped modification did not change the intrinsic crystal structure of UiO-66. According to the previous report [29], the Mn element possibly combined with the UiO-66 framework. Three dominating peaks at $2\theta = 7.3^\circ$, 8.5° and 25.8° were displayed in the XRD pattern, which were related to the (111), (200) and (442) crystal planes of UiO-66, respectively. Notably, after adsorption removal of TC and Cr(VI), the position of main peaks of MnUiO-66 performed no shift, suggesting the adsorptive behavior caused no change for the phase of MnUiO-66.

As the field emission scanning electron microscopy (FESEM) images showed in Fig. 2a, the bare UiO-66 sample performed an agglomerated nanocrystal shape and with an average diameter of 300 nm. However, after Mn-doped modification, the obtained MnUiO-66 sample presented a well-defined and dispersive cubic morphology (Fig. 2b). The modified MnUiO-66 had a smaller size of 200 nm than pristine UiO-66. EDS elemental mapping spectrum of MnUiO-66 was obtained using the FESEM. The C, O, Zr and Mn element mappings were showed in Fig. 2d–g, the O, Zr and Mn mappings were consistent with the C mapping, suggesting the Mn element was uniformly distributed on the framework and the results proved again that the MnUiO-66 was successfully fabricated. Moreover, the energy-dispersive X-ray spectroscopy (EDS) analysis showed that the average content of C, O, Zr and Mn were 46.11%, 30.56%, 22.13% and 1.2%, respectively. It was hard for metal ions to be doped into framework, which was the reason of low Mn content. According to the inductively coupled plasma-atomic emission spectrometry (ICP-AES) result, the Mn content in the MnUiO-66 sample was only 1.06 wt%, which confirmed the EDS analysis.

Fourier transform infrared spectroscopy (FT-IR) spectrum of UiO-66 and MnUiO-66 samples were nearly the same, further proving the functional groups of pure UiO-66 crystal was not changed but became stronger and broader by the addition of the Mn dopant (Fig. 3a). The peaks at 450 – 750 cm^{-1} belonged to $-\text{OH}$ and $\text{C}-\text{H}$ stretching and $\text{Zr}-\text{O}$ vibration occurred at 1100 cm^{-1} . The peaks at around 1580 cm^{-1} and 1430 cm^{-1} were the vibrations of $\text{O}=\text{C}-\text{O}-$ group, which proved the

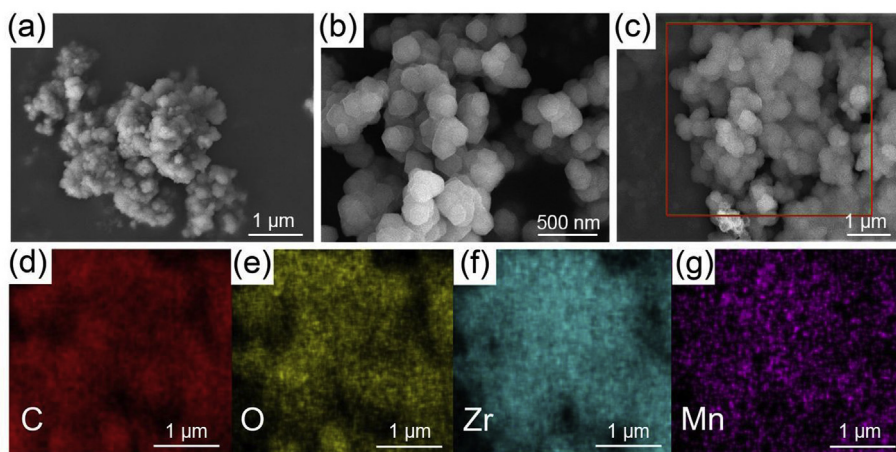


Fig. 2. FESEM images of UiO-66 (a) and MnUiO-66 (b and c) samples and EDS mappings of the portion selected: distribution of C (d), O (e), Zr (f) and Mn (g).

existence of the dicarboxylate in the framework. Obviously, there was a strong and broad band at 3450 cm^{-1} due to O–H groups in H_2O condensed in the cavities [22]. After Mn-doped modification, the adsorption peak at 3450 cm^{-1} was stronger and broader, the Mn-doped modification may increase the pore size of UiO-66, which was beneficial to water condensed.

Thermogravimetric analysis (TGA) of pristine UiO-66 and MnUiO-66 samples exhibited a weight loss of 65.52% and 68.24% at $800\text{ }^\circ\text{C}$ under nitrogen gas (N_2), respectively (Fig. 3b). Obviously, the weight loss could be divided into two successive stages. The first stage ($25\text{ }^\circ\text{C}$ – $400\text{ }^\circ\text{C}$) was supposed to the loss of guest solvent molecules (including H_2O and DMF molecules) [30]. As for the first stage, the weight loss of UiO-66 and MnUiO-66 were 29.69% and 41.42%, respectively. The Mn-doped modification made for solvent molecules (including H_2O molecules) condensed in the cavities of the framework, as confirmed by the FT-IR results. The second stage between $400\text{ }^\circ\text{C}$ and $800\text{ }^\circ\text{C}$ displayed a larger weight loss of UiO-66 (35.83%) than MnUiO-66 (26.82%). In this stage, the framework was collapsed and the metallic oxide (ZrO_2 and MnO) was produced. The residual solids were ZrO_2 of UiO-66 or a mixture of ZrO_2 and MnO of MnUiO-66, the less residual solids of MnUiO-66 implied the Mn element was successfully doped into UiO-66. Notably, the MnUiO-66 showed similar thermal stability as pristine UiO-66, suggesting that the doped-Mn was chemically coordinated to the UiO-66 host and did not form metallic oxide [31].

Good stability, large surface area and high porosity were beneficial to adsorption performance. As the TGA results showed, MnUiO-66 displayed an excellent structural stability under $400\text{ }^\circ\text{C}$. The parameters of surface area, pore size and pore volume (V_t) of UiO-66 and MnUiO-66 were assessed by the Brunauer-Emmett-Teller (BET) analysis. Fig. 4

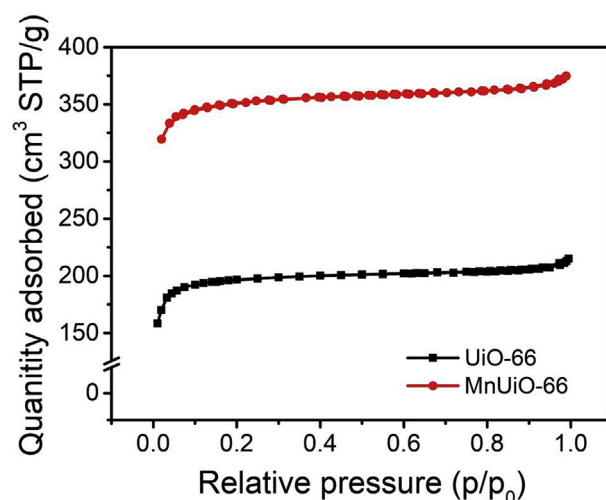


Fig. 4. The N_2 adsorption-desorption isotherms of UiO-66 and MnUiO-66 samples.

showed that both of UiO-66 and MnUiO-66 were the typical type I isotherms which reflected a volume filling theory of micropores. As Table 1 listed, the calculated BET surface area and pore size of UiO-66 were $582.34\text{ m}^2\text{ g}^{-1}$ and 1.35 nm , respectively. However, the MnUiO-66 possessed an increased BET surface area and pore size of $791.18\text{ m}^2\text{ g}^{-1}$ and 1.68 nm , respectively. The V_t was almost unchanged after Mn-doped modification. Nevertheless, a larger BET surface area

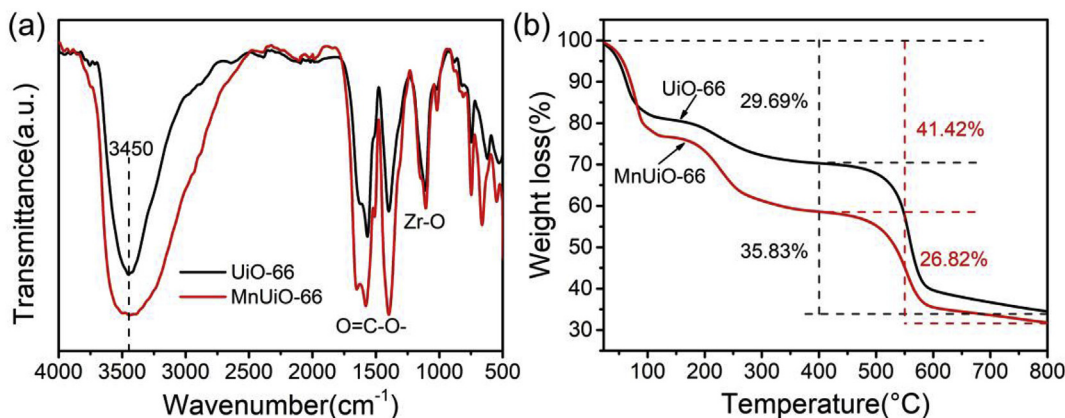


Fig. 3. FT-IR (a) and TGA (b) analyses of UiO-66 and MnUiO-66 samples.

Table 1
Surface area, pore size and pore volume parameters of UiO-66 and MnUiO-66.

Samples	Surface area ^a (m ² g ⁻¹)	Pore size ^b (nm)	V _t ^c (m ³ g ⁻¹)
UiO-66	582.34	1.35	0.34
MnUiO-66	797.18	1.68	0.33

^a Measured using N₂ adsorption with the Brunauer–Emmett–Teller (BET) method.

^b Pore size in diameter calculated by the desorption data using Barrett–Joyner–Halenda (BJH) method.

^c Total pore volume determined at P/P₀ = 0.99.

and pore size of MnUiO-66 made for the adsorption process. The larger pore size of MnUiO-66 may result in more H₂O molecules condensed in the cavities, which confirmed the FT-IR and TGA results. In summary, the Mn-doped modification made a difference to BET surface area and pore structure of UiO-66.

3.2. Adsorption studies

Adsorption performance for TC and Cr(VI) was described by the adsorption capacity of adsorbents. Therefore, a time range of 0–1440 min was applied for TC and Cr(VI) adsorption by UiO-66 and MnUiO-66 (Fig. 5). A fast adsorption was observed during the first 10 min and then acted as a tardy adsorption process. The adsorption equilibrium point was obtained at 60 min for UiO-66 and MnUiO-66. After 1440 min, the maximum adsorption capacities of UiO-66 were 12.2 mg g⁻¹ (TC) and 8.1 mg g⁻¹ (Cr(VI)) respectively, while the maximum adsorption capacities of MnUiO-66 were 72.5 mg g⁻¹ (TC) and 25.1 mg g⁻¹ (Cr(VI)) respectively. The Mn-doped modification greatly improved the adsorption performance of UiO-66. The doped Mn element possibly incorporated into the UiO-66 framework and donated its valence electrons, which caused more adsorptive sites and enhanced the adsorption performance [26,32].

3.2.1. Effect of pH values

Effect of pH value on adsorption ability of MnUiO-66 and the corresponding adsorption mechanism based on zeta potential measurements were investigated (Fig. 6). From Fig. 6a, as pH values increased from 2 to 8, the corresponding adsorption capacity of TC increased from 16.5 mg g⁻¹ to 73.5 mg g⁻¹. Obviously, the maximum adsorption capacity of MnUiO-66 for TC could be obtained at pH 8, and then the adsorption capacity slowly decreased. Anyhow, Fig. 7a showed a great adsorption performance of MnUiO-66 for TC from pH 4 to pH 12. The adsorption capacity was not obviously affected in the pH range of 4–12, indicating the TC adsorption was occurred by the π - π interaction [33]. When pH was less than 2, electrostatic repulsion force was the main

force of adsorption process due to the TC molecules and MnUiO-66 were positive charged. The zeta potential measurements of the MnUiO-66 showed that the point of zero charge (pH_{pzc}) (ca. 9.85) could be obtained in water. However, the pH_{pzc} of MnUiO-66 in water shifted to pH_{pzc} (ca. 11.15) in TC solution. The improved pH_{pzc} probably because the formation of hydrogen-bond interaction between the organic link of MnUiO-66 and benzene ring of TC [34].

From Fig. 6b, as the pH value increased from 2 to 6, Cr(VI) adsorption capacity increased, then dropped off at pH 6, at which point the optimal adsorption capacity of 25.4 mg g⁻¹ could be reached. The mechanism of Cr(VI) adsorption onto MnUiO-66 may be the strong electrostatic attraction between oxidative Cr(VI) ions and oxygen atoms of the organic linkers for the Cr(VI) adsorption was strongly affected by pH value [2]. On the basis of zeta potential measurement results, the surface charge of MnUiO-66 in Cr(VI) solution was kept positive in the pH range of 2–6, while was negative when the solution pH increased to 12. However, in the pH range of 2–12, Cr(VI) existed in anionic forms, including HCrO₄⁻ and Cr₂O₇²⁻ (2 < pH < 6) and CrO₄²⁻ (pH > 7) [35]. In the pH range of 2–6, electrostatic attraction was in dominant while the pH value was more than 6, the electrostatic repulsion hindered the adsorption process. Moreover, the MnUiO-66 pH_{pzc} of ca. 9.85 in water was lower than pH_{pzc} of ca. 7.11 in Cr(VI) solution. The lower pH_{pzc} probably due to the accumulation of negative charge in Cr(VI) solution [36]. In addition, the Eh value of Cr(VI) solution with various pH value was investigated, too. As shown Fig. S3, the Eh values decreased from 505 mV to 431 mV as the pH values increased from 2 to 6. In the pH range of 6–12, the Eh value of Cr(VI) solution increased slightly (from 431 mV to 440 mV) as pH value increased. Interestingly, the trend of the Eh value Cr(VI) solution and adsorption capacity were similar. Thus, high redox levels had a negative effect on Cr(VI) adsorption.

3.2.2. Effect of solution concentrations and coexisting ions

TC and Cr(VI) adsorption experiments with different initial solution concentrations by MnUiO-66 were conducted without adjusting pH value (the pH value of TC was 5.37 and the pH value of Cr(VI) was 5.71). As showed in Fig. 7a, the TC adsorption capacities increased quickly from 19.39 mg g⁻¹ to 184.49 mg g⁻¹, as the initial TC concentrations increased from 5 to 70 mg L⁻¹. Similarly, the adsorption capacities (from 3.32 mg g⁻¹ to 32.77 mg g⁻¹) increased as the Cr(VI) concentrations increased (from 1 mg L⁻¹ to 30 mg L⁻¹) (Fig. 7b). Generally, a higher initial solution concentration caused a higher concentration gradient driving force [37], which could be the reason for the higher adsorption capacity. Obviously, less than 30 min, the MnUiO-66 adsorbent could completely remove TC molecules and Cr(VI) at a relatively low concentration, which was conducive to industrial wastewater treatment.

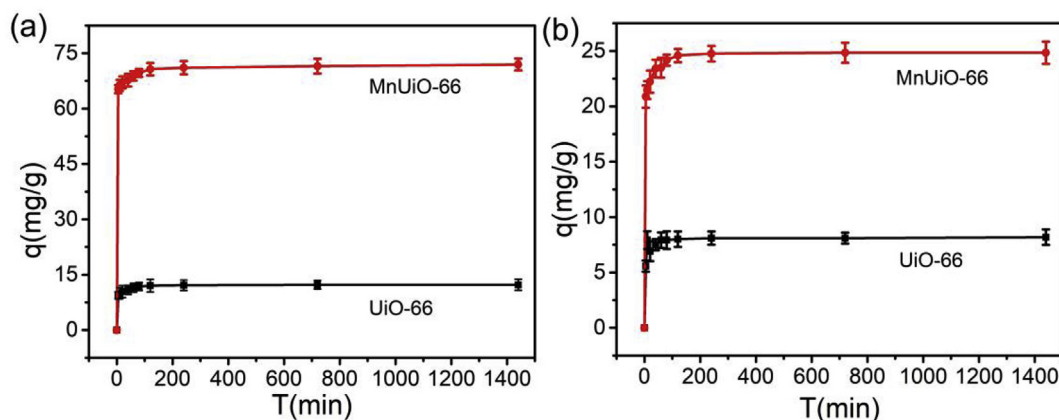


Fig. 5. Adsorption performance of UiO-66 and MnUiO-66 for TC (a) and Cr(VI) (b) (Experimental conditions: initial TC concentration = 20 mg L⁻¹; initial Cr(VI) concentration = 10 mg L⁻¹; m = 30 mg; V = 100 mL).

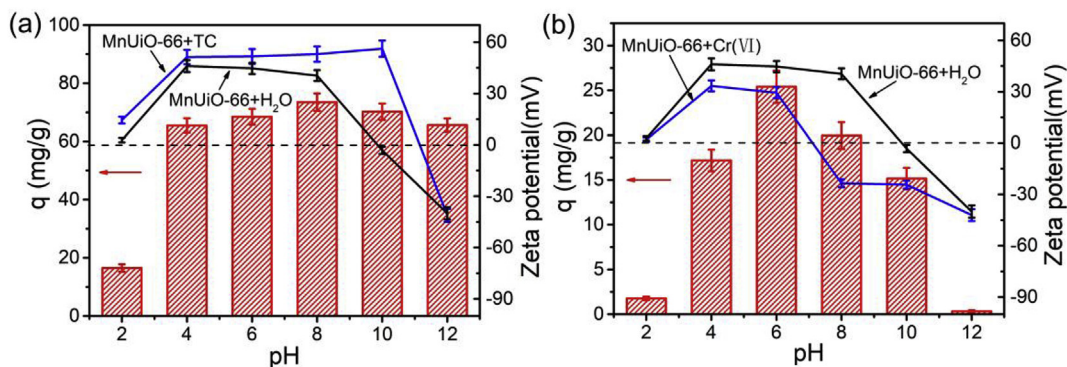


Fig. 6. Effects of pH values of TC (a) and Cr(VI) (b) solutions on adsorption performance and zeta potentials of MnUiO-66 (Experimental conditions: initial TC concentration = 20 mg L⁻¹; initial Cr(VI) concentration = 10 mg L⁻¹; m = 30 mg; V = 100 mL).

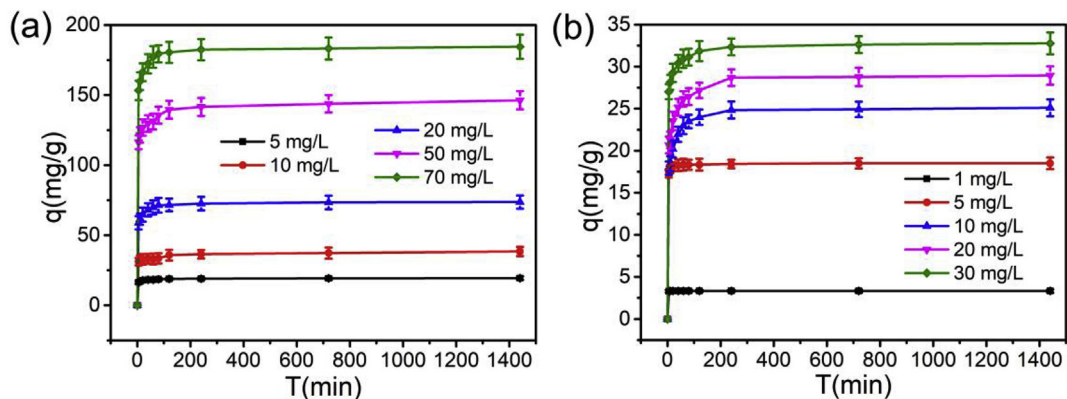


Fig. 7. Effects of different initial TC (a) and Cr(VI) (b) concentrations on the adsorption performance of MnUiO-66 (Experimental conditions: m = 30 mg; V = 100 mL).

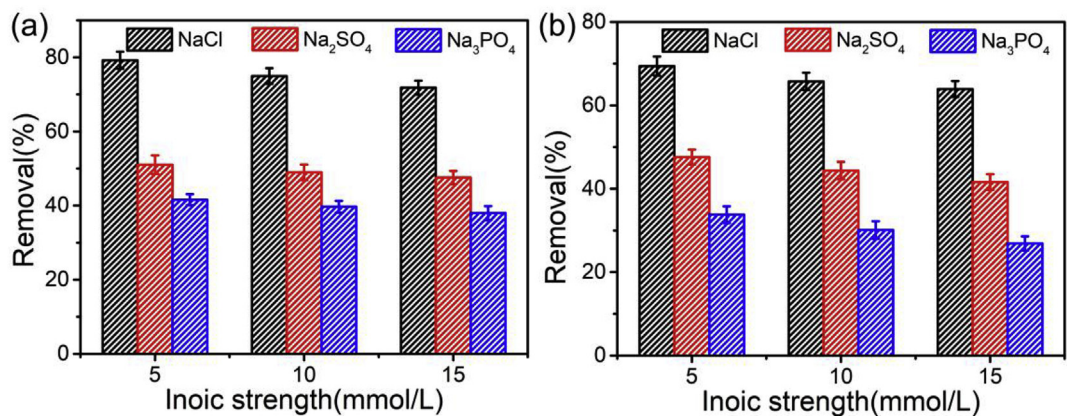


Fig. 8. Effects of coexisting ions on adsorption performance of MnUiO-66 for TC (a) and Cr(VI) (b) (Experimental conditions: initial TC concentration = 20 mg L⁻¹; initial Cr(VI) concentration = 10 mg L⁻¹; m = 30 mg; V = 100 mL).

In actual water, the TC molecules and Cr(VI) coexist with other ions, such as, Cl⁻, SO₄²⁻, PO₄³⁻. Therefore, effects of coexisting ions were investigated by adding various amount of NaCl, Na₂SO₄ and Na₃PO₄. Fig. 8 showed the ionic concentrations had an impact on the adsorptive process. As the concentrations of ions increased, the removal efficiencies of TC and Cr(VI) by MnUiO-66 decreased. The addition ions could compete the adsorptive sites of MnUiO-66 with TC molecules or Cr(VI). Notably, the negative impact of coexisting ions on TC and Cr(VI) adsorption followed the order: PO₄³⁻ > SO₄²⁻ > Cl⁻. Moreover, the anions with more negative charge could bond more strongly with the adsorbents, which could compete strongly with TC or Cr(VI).

3.2.3. Adsorption kinetic and isotherm studies

Adsorption kinetic and isotherm were studied to further understand the adsorption process. As shown in Fig. S1 and Table S1, the highest correlation coefficients (R²) of the pseudo second-order model of TC (R²: 0.997–0.999) and Cr(VI) (R²: 0.998–0.999) were obtained, which fitted better than pseudo-first-order model of TC (R²: 0.387–0.726) and Cr(VI) (R²: 0.219–0.789), and Elovich model of TC (R²: 0.673–0.945) and Cr(VI) (R²: 0.551–0.955). Therefore, chemisorption was dominant in TC and Cr(VI) adsorption reaction. Moreover, the intra-particle diffusion model suggested the plots of qt against t^{1/2} were displayed three linear sections. The first linear sections with steep slopes ((K_{id,1} (mg g⁻¹ min^{-0.5}): 5.566–49.529 for TC and K_{id,1} (mg g⁻¹ min^{-0.5}):

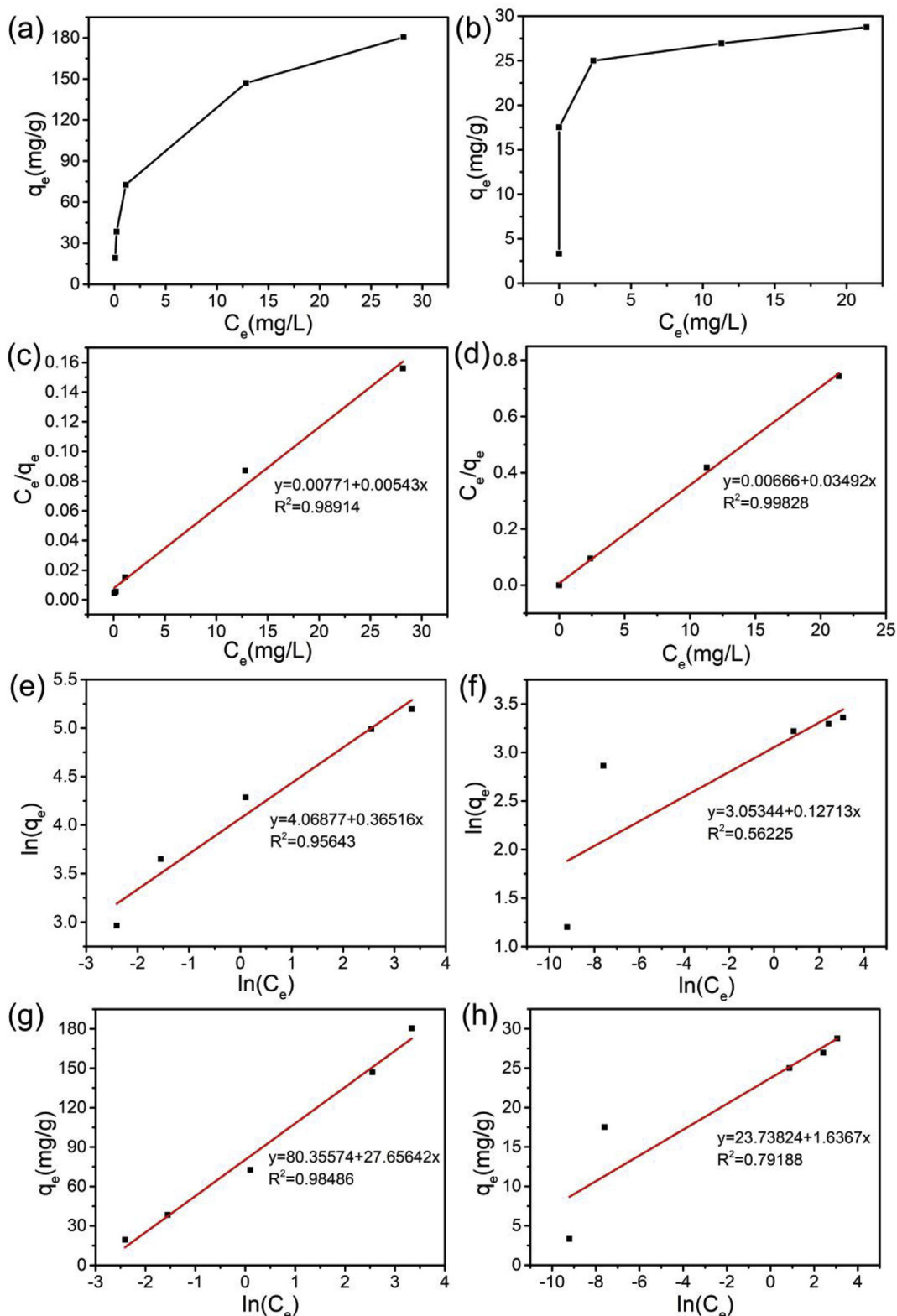


Fig. 9. Adsorption isotherms of TC (a) and Cr(VI) (b) adsorption on MnUiO-66 at 25 °C and the corresponding Langmuir fit, Freundlich fit and Temkin fit of TC (c, e and g) and Cr(VI) (d, f and h) (the values of C_e and q_e were the averages of three parallel experiments).

1.002–9.003 for Cr(VI)) indicated a rapid adsorption process. At the beginning of the adsorption reaction, there were abundant adsorption sites on MnUiO-66 surface, so that the TC and Cr(VI) could be transferred from the solution to MnUiO-66 external surface and then diffused to the internal pore structure. The second liner section with low slope

(($K_{id,2}$): 0.149–3.016 for TC and $K_{id,2}$: 0–0.744 for Cr(VI)) indicated the adsorption process andante reaching of adsorption equilibrium.

We also investigated the reaction behavior of the MnUiO-66 adsorbent towards TC and Cr(VI). Langmuir, Freundlich and Temkin models were applied to explore the adsorption mechanism. Langmuir

Table 2
Equilibrium constants for the adsorption of TC and Cr(VI) onto MnUiO-66.

Pollutants	Langmuir			Freundlich			Temkin		
	q_m	K_L	R^2	n	K_F	R^2	f	K_T	R^2
TC	184.162	0.704	0.989	2.739	58.439	0.956	2.9055	27.65642	0.98486
Cr(VI)	32.637	5.243	0.998	7.866	21.188	0.562	14.5037	1.6367	0.79188

Table 3
Thermodynamic parameters for adsorption of TC and Cr(VI) on the MnUiO-66.

Pollutants	T (K)	ΔG^0 (kJ mol ⁻¹)	ΔH^0 (kJ mol ⁻¹)	ΔS^0 (kJ mol ⁻¹ K ⁻¹)
TC	298	-9.137	71.321	0.270
	308	-11.837		
	318	-14.537		
Cr(VI)	298	-5.259	37.355	0.143
	308	-6.689		
	318	-8.119		

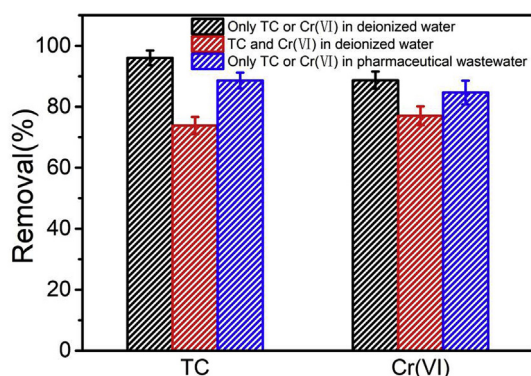


Fig. 10. The removal efficiencies of TC and Cr(VI) by MnUiO-66 in single system, mixed system and pharmaceutical wastewater (Experimental conditions: initial TC concentration = 20 mg L⁻¹; initial Cr(VI) concentration = 10 mg L⁻¹; m = 30 mg; V = 100 mL).

isotherm assumed a homogeneous surface of the adsorbent. The Freundlich isotherm was based on a heterogeneous surface with unequal binding sites. Temkin model described the interaction between adsorbent and adsorbing particles. From the Fig. 9 and Table 2, we could see that the Langmuir model had the most accordance with experiment data for the highest R^2 of TC (0.989) and Cr(VI) (0.998) in adsorption process. It suggested that every adsorption site on MnUiO-66 adsorbent had an equal adsorption energy [38].

Table 4
Comparison of the MnUiO-66 adsorbent with other materials at 298 K.

Adsorbent	Adsorption conditions			Adsorption capacity		Ref
	Adsorbent dosage (g L ⁻¹)	pH	Initial concentration (mg L ⁻¹)	TC	Cr(VI)	
MnUiO-66	0.2	No adjustment	5-70 (TC); 1-30 (Cr(VI))	184.49	32.77	This work
UiO-66	0.5	No adjustment	10-100	23.1	-	[22]
In ₂ S ₃ @MIL-125(Ti)	0.3	3.3	9.4-66.7	154.3	-	[37]
MWCNT/MIL-53(Fe)	0.2	7	1-200	364.3	-	[42]
CuCo/MIL-101	0.5	4.8	10-100	54.0	-	[43]
Fe/Zn-biochar	1	6	40-150	102.0	-	[44]
graphene oxide/calcium alginate	0.5	No adjustment	10-60	131.57	-	[45]
Cu-BTC	0.5	7	10-40	-	48	[46]
ZIF-67 microcrystals	1	No adjustment	6-15	-	13.34	[47]
Ni/Fe layered double hydroxides	0.2	No adjustment	4-20	-	26.68	[48]
Ni/Mg/Al layered double oxides	0.5	No adjustment	20-100	-	103.4	[49]
corn straw biochar	2.5	No adjustment	25-950	-	26.18	[50]

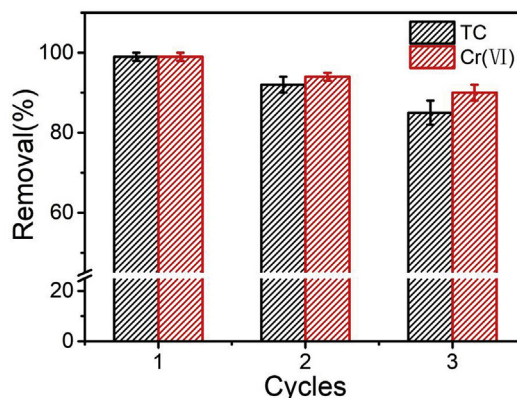


Fig. 11. The removal efficiencies of TC and Cr(VI) by MnUiO-66 over three cycles (Experimental conditions: initial TC concentration = 10 mg L⁻¹; initial Cr(VI) concentration = 5 mg L⁻¹; m = 30 mg; V = 100 mL).

3.2.4. Adsorption thermodynamic studies

Adsorption thermodynamic of adsorption process by MnUiO-66 adsorbent was studied under various temperature (298 K, 308 K and 318 K). From Fig. S2, the adsorption capacity of MnUiO-66 increased as the temperature rose, indicating the adsorption processes were endothermic in nature. To further explore the adsorption process, thermodynamic studies were performed.

$$\ln \frac{q_e}{C_e} = -\frac{\Delta H}{RT} + \frac{\Delta S}{R} \quad (1)$$

$$\Delta G = \Delta H - T\Delta S \quad (2)$$

Where ΔG_0 was the Gibbs free energy change, ΔH_0 was enthalpy change, ΔS_0 was entropy change, R (8.314 J mol⁻¹ K⁻¹) was the universal gas constant and T (K) was the absolute temperature in Kelvin. As Table 3 listed, the positive ΔH_0 manifested the adsorption reaction of TC and Cr(VI) on MnUiO-66 adsorbent was exothermic, which confirmed conclusion of Fig. S2. Generally, physisorption (ΔH_0 : 2.1–20.9 kJ mol⁻¹) and chemisorption (ΔH_0 : 20.9–418.4 kJ mol⁻¹) can be distinguished based on the ΔH_0 values [39]. In this case, the ΔH_0 values of TC and Cr(VI) adsorption were 71.321 and 37.355 kJ mol⁻¹,

respectively, which implied the chemisorption was relatively dominant in the adsorption reaction and certified the above adsorption kinetics results. The negative ΔG value implied the adsorption process was spontaneous while the positive ΔS value demonstrated the increasing disorder at the solid/liquid interface [40].

3.2.5. Adsorption experiment on TC-Cr(VI) mixed sample and pharmaceutical wastewater

The investigation on single sample (only TC or Cr(VI) in deionized water), TC-Cr(VI) mixed sample (in deionized water) and pharmaceutical wastewater were showed in Fig. 10. In the single sample, the removal efficiencies of TC and Cr(VI) by MnUiO-66 were 96.1% and 88.7%, respectively. However, the removal rates of TC and Cr(VI) in TC-Cr(VI) mixed sample were 73.1% and 77.1%, respectively. In the TC-Cr(VI) mixed sample, the TC molecules and Cr(VI) would compete for the adsorption sites, so that the removal efficiencies decreased. Additionally, pharmaceutical wastewater was used as solution to prepare the TC-containing and Cr(VI)-containing solution to test the adsorption properties of MnUiO-66. The quality parameters of the pharmaceutical wastewater were listed in Table S2. The removal efficiencies of TC and Cr(VI) in pharmaceutical wastewater were 88.6% and 84.6%, respectively. The competitive organic matters in pharmaceutical wastewater had influence on the adsorption performance of MnUiO-66 [41]. The high removal efficiencies of MnUiO-66 in removing TC and Cr(VI) indicated the great application potential of MnUiO-66 in wastewater treatment. Moreover, compared to the adsorbents from previous studies [22,37,42–50], the as-obtained MnUiO-66 showed a great performance of TC and Cr(VI) adsorption (Table 4). Obviously, the TC and Cr(VI) adsorption of MnUiO-66 were better than biochar while worse than some inorganic materials and MOF-based adsorbents. Moreover, experimental results showed the MnUiO-66 adsorbent could completely remove TC molecules and Cr(VI) at a relatively low concentration within 30 min, which was conducive to industrial wastewater treatment. This work provided a facile strategy to enhance the adsorption performance of MOF-based adsorbent and the compound of MnUiO-66 and other materials with high performance can be fabricated in the future.

3.2.6. Regeneration tests

Reusability was very significant for the commercial application of MnUiO-66 adsorbent. The MnUiO-66 adsorbent was gathered after adsorption process and soaked in NaOH solution, then replaced with DMF and sonicated. The regenerated MnUiO-66 adsorbent was washed and dried in 60 °C vacuum. Fig. 11 showed the removal efficiencies of MnUiO-66 adsorbent after three continuous adsorption-desorption cycles of TC and Cr(VI). After third cycle, the removal efficiencies of MnUiO-66 for TC and Cr(VI) were as high as 84% and 90% respectively, which suggested excellent reusability of MnUiO-66 adsorbent.

3.2.7. Possible adsorption mechanism

In a word, the adsorption process of TC and Cr(VI) on MnUiO-66 adsorbent was complicated. Firstly, the pollutant molecules transferred from solution to MnUiO-66 outer surface and then spread to the inner pore structure and finally adsorbed by MnUiO-66. The whole adsorption process could be assumed to be a monolayer adsorption and chemisorption was dominant in adsorption reaction. The Mn-doped UiO-66 exhibited a larger BET surface area and pore size, which was attributed to the physisorption process of pore/size-selective adsorption. TC adsorption on MnUiO-66 was mainly controlled by π - π and hydrogen-bond interaction. Moreover, the Zr–O cluster in MnUiO-66 with structural defect sites had some Lewis acid properties, while the amine groups in TC molecules were alkaline. The acid-alkaline interaction was also one of the chemisorption mechanisms. Nevertheless, the Cr(VI) adsorption on MnUiO-66 was dominated by the electrostatic attraction between oxidative Cr(VI) ions and oxygen atoms of the organic linkers. Besides, the strong coulombic attraction between the pores in MnUiO-

66 framework and Cr(VI) ions was also attributed to the adsorption reaction.

4. Conclusion

In a word, we fabricated the Mn-doped UiO-66 (denoted as MnUiO-66) adsorbent by a facile solvothermal method. Compared to pristine UiO-66, the MnUiO-66 exhibited no phase transition while the Mn-doped modification caused higher surface area and pore size. Moreover, the doped Mn element possibly incorporated into the UiO-66 framework and donated its valence electrons, thus caused more adsorptive sites. The TC and Cr(VI) adsorption experiments proved that the Mn-doped modification greatly improved the adsorption performance. High adsorption capacities of 184.49 mg g⁻¹ and 32.77 mg g⁻¹ were obtained for TC and Cr(VI) adsorption by MnUiO-66, respectively. The adsorption properties of MnUiO-66 were influenced by pH values, initial concentrations and coexisting ions and the adsorption mechanism based on zeta potential measurement was proposed. Adsorption kinetic and isotherm studies indicated chemisorption was dominant in TC and Cr(VI) adsorption process and the MnUiO-66 adsorbent had a homogenous surface for adsorption. Adsorption thermodynamic studies suggested the TC and Cr(VI) adsorption on MnUiO-66 were spontaneous and exothermic. More importantly, the MnUiO-66 could efficiently remove TC and Cr(VI) from TC-Cr(VI) mixed system and pharmaceutical wastewater. We hope that the above results could provide a valuable strategy to develop effective MOF-based adsorbent for removal of contaminants in aquatic environment.

Acknowledgements

The study was financially supported by the National Natural Science Foundation of China (Grant No. 51578223, 51521006 and 51709103), the Key Research and Development Program of Hunan Province (Grant No. 2017SK2242) and China Postdoctoral Science Foundation (Grant No. 2018M630901).

Appendix A. Supplementary data

Supplementary data to this article can be found online at <https://doi.org/10.1016/j.micromeso.2018.11.014>.

References

- [1] B. Peng, L. Tang, G. Zeng, S. Fang, X. Ouyang, B. Long, Y. Zhou, Y. Deng, Y. Liu, J. Wang, Self-powered photoelectrochemical aptasensor based on phosphorus doped porous ultrathin g-C₃N₄ nanosheets enhanced by surface plasmon resonance effect, *Biosens. Bioelectron.* 121 (2018) 19–26.
- [2] P.A. Kobielska, A.J. Howarth, O.K. Farha, S. Nayak, Metal-organic frameworks for heavy metal removal from water, *Coord. Chem. Rev.* 358 (2018) 92–107.
- [3] Y. Yang, Z. Zeng, C. Zhang, D. Huang, G. Zeng, R. Xiao, C. Lai, C. Zhou, H. Guo, W. Xue, Construction of iodine vacancy-rich BiOI/Ag@AgI Z-scheme heterojunction photocatalysts for visible-light-driven tetracycline degradation: transformation pathways and mechanism insight, *Chem. Eng. J.* 349 (2018) 808–821.
- [4] S.R. Batten, N.R. Champness, X.M. Chen, J. Garciamartinez, S. Kitagawa, L. Öhrström, M. O'Keefe, M. Paik Suh, J. Reedijk, Terminology of metal-organic frameworks and coordination polymers (IUPAC Recommendations 2013), *Pure Appl. Chem.* 85 (2013) 1715–1724.
- [5] O.M. Yaghi, G. Li, H. Li, Selective binding and removal of guests in a microporous metal-organic framework, *Nature* 378 (1995) 703–706.
- [6] O.K. Farha, I. Eryazici, N.C. Jeong, B.G. Hauser, C.E. Wilmer, A.A. Sarjeant, R.Q. Snurr, S.B.T. Nguyen, A.Ö. Yazaydin, J.T. Hupp, Metal-organic framework materials with ultrahigh surface areas: is the sky the limit? *J. Am. Chem. Soc.* 134 (2012) 15016–15021.
- [7] E. Haque, J.E. Lee, I.T. Jang, Y.K. Hwang, J.-S. Chang, J. Jegal, S.H. Jung, Adsorptive removal of methyl orange from aqueous solution with metal-organic frameworks, porous chromium-benzenedicarboxylates, *J. Hazard Mater.* 181 (2010) 535–542.
- [8] F. Tan, L. Min, K. Li, Y. Wang, J. Wang, X. Guo, G. Zhang, C. Song, Facile synthesis of size-controlled MIL-100(Fe) with excellent adsorption capacity for methylene blue, *Chem. Eng. J.* 281 (2015) 360–367.
- [9] E. Haque, J.W. Jun, S.H. Jung, Adsorptive removal of methyl orange and methylene blue from aqueous solution with a metal-organic framework material, *iron*

- terephthalate (MOF-235), *J. Hazard Mater.* 185 (2011) 507–511.
- [10] Q. Yang, S. Ren, Q. Zhao, R. Lu, C. Hang, Z. Chen, H. Zheng, Selective separation of methyl orange from water using magnetic ZIF-67 composites, *Chem. Eng. J.* 333 (2018) 49–57.
- [11] Y. Peng, Y. Zhang, H. Huang, C. Zhong, Flexibility induced high-performance MOF-based adsorbent for nitroimidazole antibiotics capture, *Chem. Eng. J.* 333 (2018) 678–685.
- [12] Q.R. Fang, D.Q. Yuan, J. Sculley, J.R. Li, Z.B. Han, H.C. Zhou, Functional mesoporous metal-organic frameworks for the capture of heavy metal ions and size-selective catalysis, *Inorg. Chem.* 49 (2010) 11637–11642.
- [13] A. Maleki, B. Hayati, M. Naghizadeh, W.J. Sang, Adsorption of hexavalent chromium by metal organic frameworks from aqueous solution, *J. Ind. Eng. Chem.* 28 (2015) 211–216.
- [14] Y. Bai, Y. Dou, L.H. Xie, W. Rutledge, J.R. Li, H.C. Zhou, ChemInform Abstract: Zr-based metal-organic frameworks: design, synthesis, structure, and applications, *Chem. Soc. Rev.* 47 (2016) 2327–2367.
- [15] N.C. Burtch, H. Jasuja, K.S. Walton, Water stability and adsorption in metal-organic frameworks, *Chem. Rev.* 114 (2014) 10575–10612.
- [16] M. Kim, S.M. Cohen, Discovery, development, and functionalization of Zr(IV)-based metal-organic frameworks, *CrystEngComm* 14 (2012) 4096–4104.
- [17] N.C. Burtch, H. Jasuja, K.S. Walton, Water stability and adsorption in metal-organic frameworks, *Chem. Rev.* 114 (2014) 10575–10612.
- [18] G.S. Cláudia, L. Ignacio, C. Avelino, G. Hermenegildo, Water stable Zr-benzenedicarboxylate metal-organic frameworks as photocatalysts for hydrogen generation, *Chemistry* 16 (2010) 11133–11138.
- [19] Q. Yang, A.D. Wiersum, P.L. Llewellyn, V. Guillermin, C. Serre, G. Maurin, Functionalizing porous zirconium terephthalate UiO-66(Zr) for natural gas upgrading: a computational exploration, *Chem. Commun.* 47 (2011) 9603–9605.
- [20] J. Cao, Z.-h. Yang, W.-p. Xiong, Y.-y. Zhou, Y.-r. Peng, X. Li, C.-y. Zhou, R. Xu, Y.-r. Zhang, One-step synthesis of Co-doped UiO-66 nanoparticle with enhanced removal efficiency of tetracycline: simultaneous adsorption and photocatalysis, *Chem. Eng. J.* 353 (2018) 126–137.
- [21] H. Molavi, A. Hakimian, A. Shojaei, M. Raeeszadeh, Selective dye adsorption by highly water stable metal-organic framework: long term stability analysis in aqueous media, *Appl. Surf. Sci.* 445 (2018) 424–436.
- [22] C. Chen, D. Chen, S. Xie, H. Quan, X. Luo, L. Guo, Adsorption behaviors of organic micropollutants on zirconium metal-organic framework UiO-66: analysis of surface interactions, *ACS Appl. Mater. Interfaces* 9 (2017) 41043–41054.
- [23] T. He, Y.-Z. Zhang, X.-J. Kong, J. Yu, X.-L. Lv, Y. Wu, Z.-J. Guo, J.-R. Li, Zr(IV)-based metal-organic framework with T-shaped ligand: unique structure, high stability, selective detection, and rapid adsorption of $\text{Cr}_2\text{O}_7^{2-}$ in water, *ACS Appl. Mater. Interfaces* 10 (2018) 16650–16659.
- [24] H. Saleem, U. Rafique, R.P. Davies, Investigations on post-synthetically modified UiO-66-NH₂ for the adsorptive removal of heavy metal ions from aqueous solution, *Microporous Mesoporous Mater.* 221 (2016) 238–244.
- [25] J.M. Yang, R.J. Ying, C.X. Han, Q.T. Hu, H.M. Xu, J.H. Li, Q. Wang, W. Zhang, Adsorptive removal of organic dyes from aqueous solution by a Zr-based metal-organic framework: effects of Ce(III) doping, *Dalton Trans.* 47 (2018) 3913–3920.
- [26] Z. Li, Y. Sun, J. Xing, Y. Xing, A. Meng, One step synthesis of Co/Cr-codoped ZnO nanoparticle with superb adsorption properties for various anionic organic pollutants and its regeneration, *J. Hazard Mater.* 352 (2018) 204–214.
- [27] C. Fu, H. Zhou, L. Tan, Z. Huang, Q. Wu, X. Ren, J. Ren, X. Meng, Microwave-activated Mn-doped zirconium metal-organic framework nanocubes for highly effective combination of microwave dynamic and thermal therapies against cancer, *ACS Nano* 12 (2018) 2201–2210.
- [28] Y. Wu, X. Li, Q. Yang, D. Wang, Q. Xu, F. Yao, F. Chen, Z. Tao, X. Huang, Hydrated lanthanum oxide-modified diatomite as highly efficient adsorbent for low-concentration phosphate removal from secondary effluents, *J. Environ. Manag.* 231 (2019) 370–379.
- [29] A.M. Ebrahim, T.J. Bandoz, Ce(III) doped Zr-based MOFs as excellent NO₂ adsorbents at ambient conditions, *ACS Appl. Mater. Interfaces* 5 (2013) 10565–10573.
- [30] N. E. R. T. M. D. M.M. A. Ethylene diamine grafted nanoporous UiO-66 as an efficient basic catalyst in the multi-component synthesis of 2-aminithiophenes, *Appl. Organomet. Chem.* 32 (2018) e4307.
- [31] Z. Ding, X. Chen, M. Antonietti, X. Wang, Synthesis of transition metal-modified carbon nitride polymers for selective hydrocarbon oxidation, *ChemSuschem* 4 (2015) 274–281.
- [32] N.T.T. Ha, O.V. Lefedova, N.N. Ha, Theoretical study on the adsorption of carbon dioxide on individual and alkali-metal doped MOF-5s, *Russ. J. Phys. Chem.* 90 (2016) 220–225.
- [33] M. Oveisi, M.A. Asli, N.M. Mahmoodi, MIL-Ti metal-organic frameworks (MOFs) nanomaterials as superior adsorbents: synthesis and ultrasound-aided dye adsorption from multicomponent wastewater systems, *J. Hazard Mater.* 347 (2018) 123–140.
- [34] D. Mitrogiannis, M. Psychoyou, I. Baziotis, V.J. Inglezakis, N. Koukouzas, N. Tsoukalas, D. Palles, E. Kamitsos, G. Oikonomou, G. Markou, Removal of phosphate from aqueous solutions by adsorption onto Ca(OH)₂ treated natural clinoptilolite, *Chem. Eng. J.* 320 (2017) 520–522.
- [35] J. Zhu, S. Wei, H. Gu, S.B. Rapole, Q. Wang, Z. Luo, N. Haldolaarachchige, D.P. Young, Z. Guo, One-pot synthesis of magnetic graphene nanocomposites decorated with core@double-shell nanoparticles for fast chromium removal, *Environ. Sci. Technol.* 46 (2012) 977–985.
- [36] R. Xu, M. Zhang, R.J. Mortimer, G. Pan, Enhanced phosphorus locking by novel lanthanum/aluminum-hydroxide composite: implication for eutrophication control, *Environ. Sci. Technol.* 51 (2017) 3418–3425.
- [37] W. Hou, X. Yuan, W. Yan, G. Zeng, H. Dong, X. Chen, L. Leng, Z. Wu, L. Peng, In situ synthesis of In₂S₃@MIL-125(Ti) core-shell microparticle for the removal of tetracycline from wastewater by integrated adsorption and visible-light-driven photocatalysis, *Appl. Catal. B Environ.* 186 (2016) 19–29.
- [38] K.Y. Shin, J.Y. Hong, J. Jang, Heavy metal ion adsorption behavior in nitrogen-doped magnetic carbon nanoparticles: isotherms and kinetic study, *J. Hazard Mater.* 190 (2011) 36–44.
- [39] Z. Wu, H. Zhong, X. Yuan, H. Wang, L. Wang, X. Chen, G. Zeng, Y. Wu, Adsorptive removal of methylene blue by rhamnolipid-functionalized graphene oxide from wastewater, *Water Res.* 67 (2014) 330–344.
- [40] W. Xiong, G. Zeng, Z. Yang, Y. Zhou, C. Zhang, M. Cheng, Y. Liu, L. Hu, J. Wan, C. Zhou, Adsorption of tetracycline antibiotics from aqueous solutions on nanocomposite multi-walled carbon nanotube functionalized MIL-53(Fe) as new adsorbent, *Sci. Total Environ.* 627 (2018) 235–244.
- [41] C. Fei, Y. Qi, Z. Yu, H. An, J. Zhao, T. Xie, Q. Xu, X. Li, D. Wang, G. Zeng, Photo-reduction of bromate in drinking water by metallic Ag and reduced graphene oxide (RGO) jointly modified BiVO₄ under visible light irradiation, *Water Res.* 101 (2016) 555–563.
- [42] W. Xiong, G. Zeng, Z. Yang, Y. Zhou, C. Zhang, M. Cheng, Y. Liu, L. Hu, J. Wan, C. Zhou, R. Xu, X. Li, Adsorption of tetracycline antibiotics from aqueous solutions on nanocomposite multi-walled carbon nanotube functionalized MIL-53(Fe) as new adsorbent, *Sci. Total Environ.* 627 (2018) 235–244.
- [43] J. Jin, Z. Yang, W. Xiong, Y. Zhou, R. Xu, Y. Zhang, J. Cao, X. Li, C. Zhou, Cu and Co nanoparticles co-doped MIL-101 as a novel adsorbent for efficient removal of tetracycline from aqueous solutions, *Sci. Total Environ.* 650 (2019) 408–418.
- [44] Y. Zhou, X. Liu, Y. Xiang, P. Wang, J. Zhang, F. Zhang, J. Wei, L. Luo, M. Lei, L. Tang, Modification of biochar derived from sawdust and its application in removal of tetracycline and copper from aqueous solution: adsorption mechanism and modelling, *Bioresour. Technol.* 245 (2017) 266–273.
- [45] H. Zhu, T. Chen, J. Liu, D. Li, Adsorption of tetracycline antibiotics from an aqueous solution onto graphene oxide/calcium alginate composite fibers, *RSC Adv.* 8 (2018) 2616–2621.
- [46] A. Maleki, B. Hayati, M. Naghizadeh, S.W. Joo, Adsorption of hexavalent chromium by metal organic frameworks from aqueous solution, *J. Ind. Eng. Chem.* 28 (2015) 211–216.
- [47] X. Li, X. Gao, L. Ai, J. Jiang, Mechanistic insight into the interaction and adsorption of Cr(VI) with zeolitic imidazolate framework-67 microcrystals from aqueous solution, *Chem. Eng. J.* 274 (2015) 238–246.
- [48] Y. Lu, B. Jiang, L. Fang, F. Ling, J. Gao, F. Wu, X. Zhang, High performance NiFe layered double hydroxide for methyl orange dye and Cr(VI) adsorption, *Chemosphere* 152 (2016) 415–422.
- [49] C. Lei, X. Zhu, B. Zhu, C. Jiang, Y. Le, J. Yu, Superb adsorption capacity of hierarchical calcined Ni/Mg/Al layered double hydroxides for Congo red and Cr(VI) ions, *J. Hazard Mater.* 321 (2017) 801–811.
- [50] N. Zhao, Z. Yin, F. Liu, M. Zhang, Y. Lv, Z. Hao, G. Pan, J. Zhang, Environmentally persistent free radicals mediated removal of Cr(VI) from highly saline water by corn straw biochars, *Bioresour. Technol.* (2018) 294–301.